STRESS–BASED TORQUE AND DRAG MODEL

A Thesis

by

HAMZA MANSOURI

Submitted to the Office of Graduate and Professional Studies of
Texas A&M University
in partial fulfillment of the requirements for the degree of

MASTER OF SCIENCE

Chair of Committee,	Samuel F. Noynaert
Committee Members,	Jerome Schubert
	Maria Barrufet
Head of Department,	Daniel Hill

August 2017

Major Subject: Petroleum Engineering

ABSTRACT

The models used currently in industry have shown a considerable discrepancy between theoretical data and actual data observed in the field. The birth of torque and drag (T&D) modeling was in 1984 in Exxon Production Research Company, and was published by C.A Johancsik. It provided the first mechanical model as well as an illustration of the origin of torque and drag forces. Johancsik's paper stated that these resisting forces originate from the friction of the drill string against the wellbore and depend on the drill string weight supported by the borehole. Many subsequent models adopted the same concept including some improvements.

In this work, a new approach of torque and drag calculation is proposed. It consists of taking the forces acting on the drill string and converting them into resulting stresses on the pipe body, and transferring the stress tensor from one segment to the next using continuum mechanics geometrical transformations. The stress tensors are accumulated to yield the resulting stress acting on an element of the drill string in a given depth of the well. The back calculation from stress to forces allows deriving the cumulative traction and compression forces, and thus drag and torque. This approach has two main advantages over the discrete method proposed by Johancsik. First, when a force is applied on a body it propagates through the body, therefore, even if the force is axial, a portion of it is going to act normally and vice versa. Consequently, the axial force Johancsik is calculating does not fully act in the same axis, and the same can be said about the forces in the other directions. In this case, it is more physically representative to base the analysis on stress

and not forces. Second, continuum mechanics provides a sound tool in handling geometries through stress tensor transformation matrices used in our model, instead of the angular approximations for inclination and azimuth used in Johancsik's equations.

A comparison between the two models for a real field case is included to show the relative under-prediction of the old model compared to the proposed model and actual data.

DEDICATION

This thesis is dedicated to my parents, my sister and my brother for their support and encouragement. Only through God and family support, I was able to finish this work.

AKNOWLEDGEMENTS

I would like to thank my advisor Dr. Sam Noynaert and professor Fred Dupriest for their guidance and great discussions during the work on the thesis, and for their helpful insights about the subject of this thesis. My thanks go to all the faculty and staff at Harold Vance department of petroleum engineering for their different contributions to this work both academically and logistically, as well as Texas A&M University. Finally, I would like to thank all my friends and fellow Aggies for all the great times we have had for the years I have spent on campus.

CONTRIBUTORS AND FUNDING SOURCES

This work was supervised by a thesis committee consisting of Professor Samuel F. Noynaert as advisor and committee chair and Professors Jerome Schubert and Maria Barrufet of the Department of Petroleum Engineering.

All work for the thesis was completed independently by the student.

This work was entirely made possible by the Fulbright Grant. Its contents are solely the responsibility of the authors and do not necessarily represent the official views of the Fulbright Foreign Scholarship Board.

TABLE OF CONTENTS

LIST OF FIGURES

LIST OF TABLES

CHAPTER I

INTRODUCTION AND LITERATURE REVIEW

Introduction

The number of the unknowns in the drilling business is as big as the effort that has been spent to invent and create new models to narrow down these unknowns. Torque and drag prediction was one of these unknowns until the first modeling approach was created by (Johancsik, et al. 1984) in 1984. This model set the stage for companies around the world to create their own models and software for torque and drag. As with any initial model, it had imperfections that were addressed by each company according to their operational processes. One of the major imperfections with the model used to calculate torque and drag currently is the "Friction Factor" (FF). Since the FF in Johancsik model should be estimated and back calculated using trial and error methods, it has been calibrated to include more than the physical quantity it represents. In its pure physics-based definition, "Friction Factor" is a quantity that characterizes the resistance to relative movements of two surfaces in contact depending on their respective roughness. In torque and drag modeling parlance, the friction factor has become a fudge factor or correction factor representing among others: well tortuosity, viscous drag, formation type, string stiffness and anything else that makes it more difficult to move the pipe within the wellbore.

Industry professionals have always been aware that the "Friction Factor" used in these models is just a factor that intends to correct for all the forces acting on the drill

string without being included in the equations of the models. Therefore, many researchers have attempted to purify the friction factor from all the other forces it represented. Exxon Mobil, which was home of the first model in 1984, later included a new force to add to pipe weight that accounts for the shear of drilling fluids on drillpipes. K&M included "Hydraulic lift" to account for buoyancy created by drilling fluids that affects the proportion of the pipe weight supported by the wellbore, and many other companies made similar efforts to obtain a more accurate model for torque and drag.

As the oil industry began to drill more horizontal wells, and especially after the shale boom, an ever-increasing number of companies started to plan for extended reach horizontals. They had to overcome many hurdles along the way and one of these hurdles was excessive torque and drag. The need for accurate modeling and prediction of the parameters driving toque and drag is a key to success in every drilling program. Being able to accurately account for compressive forces acting on a drill string will reflect on the ability to predict buckling zones in directional wells and adopt the appropriate remedies in order to transfer more weight to the bit and continue drilling efficiently.

Although published mechanical works have extensively studied the buckling phenomena, and set the onset criterion for both helical and sinusoidal buckling, many models adopted in the drilling industry still introduce correction factors to the buckling criterion. The goal from doing so is to meet the compressive forces they use in their convention of torque and drag model, (Mitchell, et al. 1999), (Dunayevski, et al. 1983), (Lubinski, et al. 1962).

The present work proposes a new modeling approach to calculate torque and drag through stress and strain generated by all forces acting on the drill string, taking advantage at the same time of the geometrical ease provided by stress transformations in order to overcome corrections due to inclination and azimuth changes.

The First Model for Torque and Drag in Directional Wells: Soft String Model

Many studies suggest that the theory behind the present torque and drag model originated in the 1984 paper by C.A. Johancsik (Johancsik et. al. 1984). In this model, the pipe is viewed as analogous to a heavy cable or a chain lying along the wellbore. The model ignores any tubular stiffness effect, therefore, the axial tension and torque forces are supported by the drill string, and the contact forces are supported by the wellbore.

According to Johancsik model, torque and drag contributing forces are: normal force perpendicular to the contact surface, buoyed weight of the pipe element, and friction force. Depending on the hole section where the pipe segment is located, the normal force and friction force are affected by the tension in the pipe section (straight pipe vs bending portion of pipe). The main assumption in Johancsik model is that torque and drag are entirely due to Sliding friction forces, based on that he uses Coulomb's friction model to link sliding friction force to the normal contact force via the coefficient of friction. Later on in 1987, Johancsik integrated mud pressure in the model in order to account for its effect on pipe tension, and differentiate between upward and downward pipe motion in the calculations. The model later was used to back calculate apparent friction factors and interpret hole geometry, hole cleaning problems, and to improve hydraulics. The works that followed and that adopted the same model, (Sheppard et al. 1987), (Mitchell, and

Samuel, 2009), (Adnoy, et al.,2010), (Gaynor, et al. 2002), (Mailda, and Wojtanowicz, 1987), and (Manson, et al. 2007), were focused on improving the estimation of the friction factor. (Lesage, et al. 1988) developed a computational model that averaged axial and rotational friction factors separately and other studies focused on different features of the model such as hole cleaning, mud, hydraulics, etc. Having in common the fact of adding correction factors to correlate with field data.

The soft-string modeling methodology relies on compartmentalizing the drill string into short elements joined by connections that transmit tension, compression and torsion. The equations are applied to each segment. Setting the initial conditions at the drill bit (bit torque and weight on bit) the calculations start from the bottom of the drill string and upwards to the surface. The resulting surface torque, axial drag and weight is the summation of these values from the bottom, across each pipe element and to the surface. The torque force is the moment of all forces acting tangentially on each tool joint.

It is worth mentioning that some of the major assumptions of this model is that the string is permanently in contact with the wellbore, which means that the radial clearance effects and bending moments are both ignored.

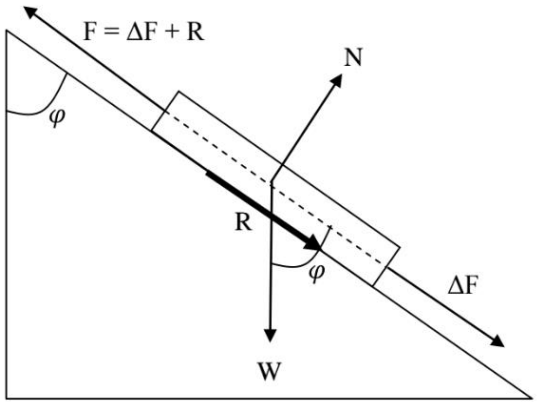

Figure 1: An Inclined Pipe Segment

Johancsik used basic Newtonian physics laws to develop the equations he presented in his paper (Johancsik, et al. 1984). It involved considering a drill pipe in static mode at first, and making the inventory of the forces acting on a portion of pipe **Figure 1**, then choosing a system of axis to project all the forces. This system of axis will be chosen in a way to make most of calculations easy. **Figure 2** and **Figure 3** present graphically the phenomena occurring at each segment in a static mode.

According to Johancsik's model, the normal force is:

$$F_N = [(F_t * \Delta\alpha \sin\theta)^2 + (F_t * \Delta\theta + W * \sin\theta)^2]^{1/2} \quad \text{Eq.1}$$

With:

F_i: downward compression force, F_{i+1}: Upward tension force, W: Weight or gravity force, F_N: Normal force, $F_{friction}$: surface friction force, α: angle between vertical W force and X_1 local axis (well inclination),

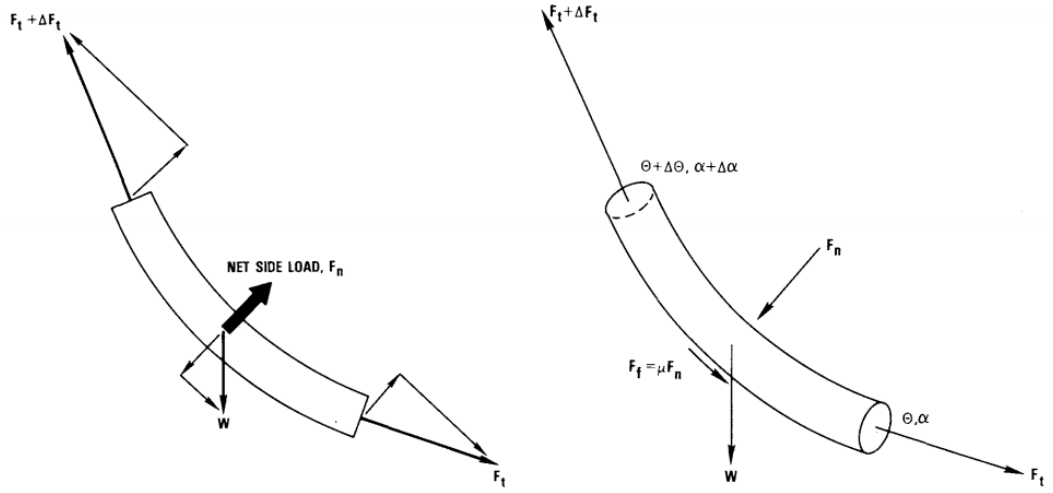

Figure 2: Loading of a Single Segment of the Drillstring

Using the friction coefficient μ, the friction resistance to pipe movement in the direction of X_1 axis is equal to:

$$F_{friction} = \mu * F_N = \mu * [(F_t * \Delta\alpha \sin\theta)^2 + (F_t * \Delta\theta + W * \sin\theta)^2]^{1/2} \quad \text{Eq.2}$$

From **Fig. 2**, Newton's law projected on X_1 yields:

$$F_{i+1} - F_i - W * \cos\alpha \ {}^{+}/_{-} \ \mu * W * \sin\alpha = 0 \quad \text{Eq.3}$$

Hence:

$$\Delta Fi = F_{i+1} - F_i = \ W * \cos\alpha \ {}^{+}/_{-} \ \mu * W * \sin\alpha \quad \text{Eq.4}$$

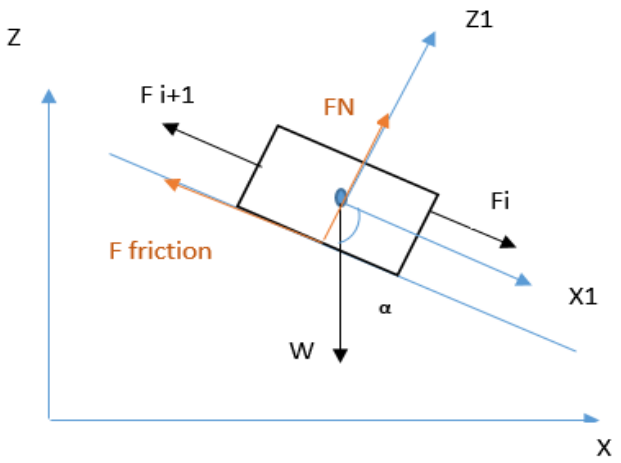

Figure 3: Force Balance Acting on a Portion of Drillstring

The +/- sign in the equation is due the change of the friction force direction. Since it is a force that opposes pipe movement it will be in the opposite direction of the two forces summation $F_{i+1} + F_{i,}$ which means that if the pipe is moving upwards i.e. $F_{i+1} \geq F_i$, then +/- in the equation is replaced by +, and vice versa.

As previously mentioned, the drag calculation is carried out in a stepwise upward process. For a drill string with *n* number of tool joints, the total drag force will be:

$$F_{drag} = \sum \Delta_{F_i} = \sum_0^n (F_{i+1} - F_i) = F_n - F_0 \qquad \text{Eq.5}$$

Where F_n is the drag force at the last tool joint at the top of the string.

Torque being the moment of the axial force, its value is given by Eq.6

$$\text{Torque} = F_{friction} * R = \mu * F_N * R = \mu * [(F_t * \Delta\alpha \sin\theta)^2 + (F_t * \Delta\theta + W * \sin\theta)^2]^{1/2} * R \qquad \text{Eq.6}$$

The whole concept is based on the geometrical representation of the vector forces acting on an element of pipe, and their projection in a local system of axis. In the plane (X_1, Z_1) the picture is shown in **Figure 3**:

Friction Factor in Johancsik Model and Continuum Mechanics

Friction factor is a key element in any T&D model, it is a dimensionless parameter that represents the roughness between the pipe body and the wellbore. Because of the complicated nature of drilling and the solid/solid contact versus the solid/fluid/solid contact between the drill pipe, the mud, and the formation or the casing, the friction factor used in T&D modeling is rather a fudge factor and in many cases, it represents one or many of the following effects.

- Pipe stiffness effect
- Viscous drag
- cuttings bed height
- Stabilizers/centralizers
- Formation type
- Pore pressure
- Circulation losses
- Wellbore breakout
- Micro-tortuosity
- Wellbore spiraling and other patterns
- Drilling fluid properties

The ranges of friction factors in T&D modeling are between 0 and 1.0 in theory but in practice generally fall between 0.05 and 0.5.

In continuum mechanics, the friction forces are defined as the forces that prevent any relative movement of two surfaces in contact to some limit before motion occurs. In this area, there are two types of friction: static friction and dynamic friction. Static friction is the frictional force that keeps an object at rest and must be overcome in order to begin movement of the object. Dynamic friction, which is more relevant for T&D modeling, is the frictional force that must be overcome to maintain the motion once it is started.

Stiff String Model

Because the two major assumptions in the soft string model are unrealistic, work followed the inception of torque and drag modeling to correct this. The following publications are representative of this effort: (Adnoy, et al, 2008), (Fazaelizadeh, et al, 2010), and (Tikhonov, et al. 2014). The stiff-string model was developed to provide a more realistic representation of both the drill string and the wellbore

This model allows initially unknown sections of the pipe not to be in contact with the wellbore. Higher contact surface between the string and the wellbore is present in curved sections of the well as opposed to straight vertical or horizontal sections of the well. The variation of contact area between drill pipe body, tool joints and stabilizers is another aspect of this consideration. These last elements of the drill string are also characterized by a higher bending moments.

It is widely accepted that the stiff-string model is more relevant in the following cases

- Highly tortuous well trajectories
- Well path with high doglegs severity
- Stiff casing jobs
- Well design with narrow radial clearances

However, this model relies on accurate values for parameters such as hole size and well trajectory that are not available in many situations. In addition, to solve for T&D using stiff string model is mathematically complicated (finite differences, finite elements and semi-analytical techniques) when attempting to properly account for the effect of hole size and radial clearances.

Finite Element Model

The key reason for the use of the finite element method is that it is able to withstand any amount of segments, which are drill string sections in our case. Therefore it is unbounded by the degree of complexity of the wellbore curvature and drill string variations (when a parameter is different isolate the hole portion and calculate again). This approach has provided a powerful tool to take into consideration the string stiffness as well as borehole/string clearance, and integrate them accurately in the torque and drag calculation model.

Starting in 1995, (Bueno, Morooka, 1995) generated a model based on the following assumption: the only contact points between the borehole and the drill string

occur at the tool joints, the wellbore was divided accordingly into contact points with specific stiffness. Later on, (Newman,, 2004) introduced the bending pipe case and improved the model with more contact points which opened the door to buckling prediction during drilling operations, then he transformed the static calculations into a dynamic time dependent model.

Pipe Buckling

Buckling is an important topic in T&D modeling. The increase of the weight supported by the wellbore when buckling occurs prevents from transmitting the weight to the bit (WOB). This is mainly due to the transformation of axial load, originally intended to be conveyed to the bit, into normal load of the drill string dissipated in the borehole walls. Buckling starts as sinusoidal deformation in the drill string. As compression builds up in the buckled portion of the string, helical buckling occurs. Ultimately, "lock-up" occurs when the buckled wellbore portion supports the entire weight rather than the bit.

There is a huge work dedicated to buckling only for its importance. Different formulas were established for the onset of both sinusoidal and helical buckling: (Dawson, Paslay, 1984), (Wu, Juvkam-Wold, 1995), (Wu, 1997), (Mitchell, 1999), (Kyllingstad, 1995). Each study from the above mentioned papers and many more have established buckling initiation criterion, for both buckling modes, sinusoidal and helical.

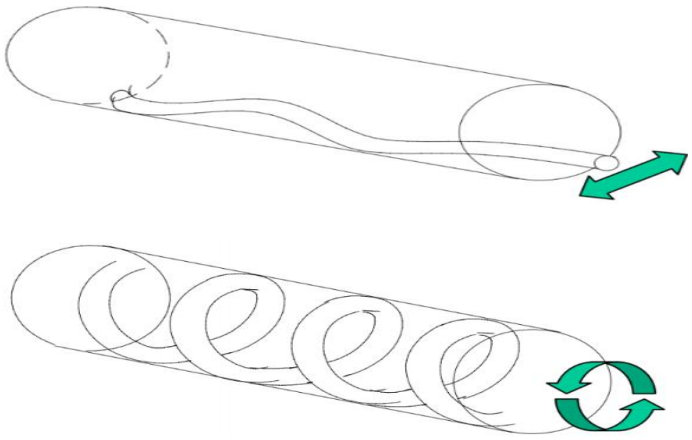

Figure 4: Sinusoidal and Helical Buckling Illustration

Figure 4 illustrates pipe buckling both sinusoidal and helical. Buckling is assessed according to the following conditions:

F<Fs No buckling

$Fs<F<\sqrt{2}Fs$ sinusoidal buckling initiated

$\sqrt{2}Fs<F<2\sqrt{2}Fs$ Helical buckling initiated

$2\sqrt{2}Fs<F$ Helical buckling

Where: F_s represents the sinusoidal buckling initiating force, F_H represents the helical buckling initiating force

Vertical Section

The first buckling model was derived by (Lubinski, et al., 1962). It evokes only sinusoidal buckling and simply states that the compressive force needed to generate this mode of deformation is:

$$F_{sin} = 1.94(EIw^2)^{1/3} \quad \text{Eq.8}$$

$$I = \frac{\pi}{64}(OD^4 - ID^4) \quad \text{Eq.9}$$

(Wu et al., 1995) introduced a sinusoidal buckling force corrected based on the previous model with the following formula:

$$F_{sin} = 2.55(EIw^2)^{1/3} \quad \text{Eq.10}$$

In addition, Wu, et al. derived the compressive force needed to generate helical buckling in the following:

$$F_{hel} = 5.55(EIw^2)^{1/3} \quad \text{Eq.11}$$

Inclined Section

Dawson and Paslay in 1984 came up with a criterion to onset of sinusoidal buckling in these sections, which requires a compressive force equal to:

$$F_{sin} = 2\left(\frac{EIw\sin\alpha}{r}\right)^{0.5} \quad \text{Eq.12}$$

With α being the section inclination and r the radial clearance.

Curved Section

In 1999, (Mitchel, 1999) derived the following formula for the onset of sinusoidal buckling in curved sections of the well:

$$F_{sin} = \frac{2Elk}{r}\left[1 + \sqrt{\frac{wsin\alpha r}{elk^2} +}\right] \quad \text{Eq.13}$$

Where:

E is Young's modulus, I is the second moment of area, w is the pipe weight, and $k = 1/R$ is build or drop, and R being the radial clearance

And

$$\mathrm{r} = \frac{1}{2}(\mathrm{ID}_{\frac{\mathrm{well}}{\mathrm{casing}}} - \mathrm{OD}_{\mathrm{tubing}}) \qquad \text{Eq.14}$$

For the helical buckling onset, the compressive force required as determined by Mitchell model is:

$$\mathrm{F}_{\mathrm{hel}} = 2.83F_{sin} \qquad \text{Eq.15}$$

CHAPTER II

FORCES ACTING ON THE DRILLSTRING

Viscous Drag or Forces due to Fluid Flow

Viscous drag is a resistive force caused mainly by viscosity and mudflow inside and outside the drill string. As the drill pipe moves inside the wellbore full of mud, the mud viscous drag will decelerate the pipe movement depending on the relative movement of both the drill string and the direction of mudflow. It should be noted that the mud flows inside and outside the drill string in opposite directions. Which means that they have opposite contribution to the forces acting on a given segment in the drill string. The fact the contact area between the mud and the drill string is different on the inside than the outside, and given that the mud velocity is also different between the inside and the outside, all make this force important in T&D modeling.

The viscous drag force for an infinite cylinder of diameter d acting on the inside body surface is given by the following formula:

$$f_D = \frac{1}{2} * C_D * \rho * \mu_0^2 * d \qquad \text{Eq.16}$$

The drag coefficient depends on the flow regime and hence on Reynold's number as follows:

if Re<100 , $C_D \sim R_e^{-1}$

if 100 < Re < 10^5 , $C_D \sim\sim 1$

If Re> $3x10^5$, C_D drops and rises, the transition corresponds to the onset of turbulent flow.

In general, C_D is related to Reynolds number according the plot in **Figure 5**:

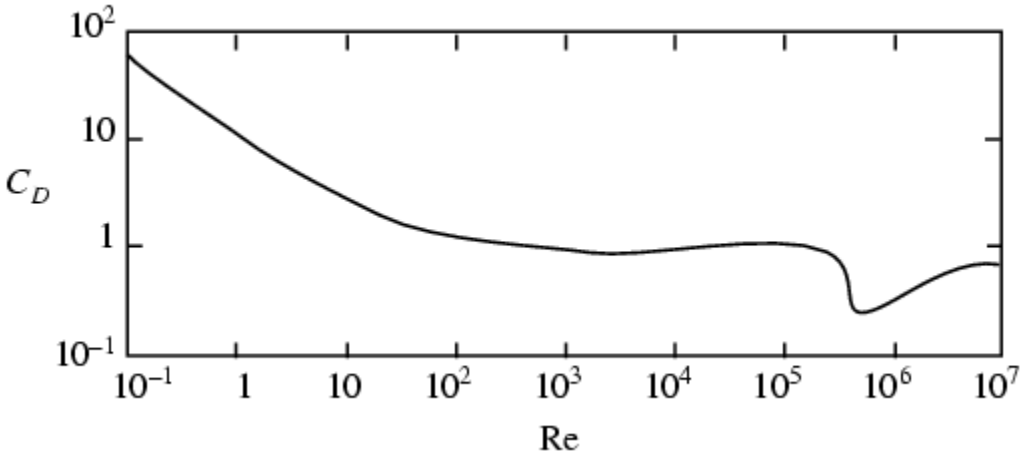

Figure 5: Viscous Drag Coefficient as a Function of Reynolds Number, (Wolfram Research, Cylinder Drag)

Similarly, the viscous drag force for an infinite cylinder of diameter d is acting on the inside body surface is:

$$f_D = \frac{1}{2} * C_D * \rho * \mu_1^2 * d_e \qquad \text{Eq.17}$$

d_e being the equivalent diameter of pipe clearance $d_e = S/\pi$, S being the clearance around the pipe inside the wellbore.

Circumference Distributed Forces

For an analysis restricted to a limited portion of pipe which is the methodology adopted to account for a cumulative T&D forces, the pipe diameter is substituted by the surface of the pipe in contact with the mud.

This surface is subject not only to the frictional viscous drag forces but also to any flow pressure outside and inside the pipe

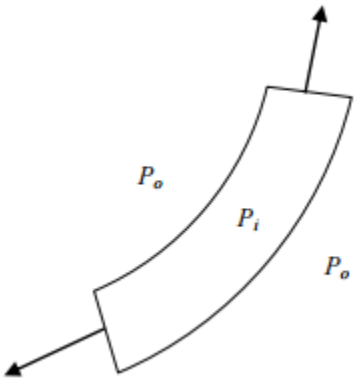

Figure 6: Pressure Acting on the Inside and Outside of the Pipe Body

The resulting force of both pressures illustrated in **Figure 6** acting on the pipe is:

$$F_p = (P_0 * S_0 - P_1 * S_1) \qquad \text{Eq.18}$$

Where:

S_0 is the circumferential area of the pipe outside, and S_1 the circumferential area of the pipe outside.

This force would not develop unless the pressures outside and inside the pipe are different or if the outer contact surface of the pipe is different from the inner area (a bent portion of drillstring).

In the case of high dogleg severity, the radius of curvature is high which drives this force higher. The curvature is an important factor in this force as it brings the far side of the pipe from the center of curvature into stretching and puts the near side under compression. This, combined with the effect of the mud weight force inside the pipe amplifies the effects of pipe bending. Study shows that these forces can be neglected and it has an accumulated effect of 4% in high depth.

Effect of Buoyancy on Gravitational Forces

The total weight of the pipe submerged in the mud should be corrected to a buoyed weight when accounting for gravitational forces:

Assuming that 95% of the string component's length is the pipe body and 5% is the tool joint, (McCormick, et al., 2011) we have:

$$W_b = W_a * (1 - MW * 7.481/490) \quad \text{Eq.18}$$

With:

$$W_{Buoy} = W_{air} - W_{fluid} \quad \text{Eq.19}$$

$$W_{fluid} = (MW * A_E) - (MW * A_I) \quad \text{E1.20}$$

$$A_E = \frac{\pi}{4} * \left(0.95 * (OD_{PB})^2 + 0.005 * \left(OD_{TJ}\right)^2\right) \quad \text{Eq.21}$$

$$A_I = \frac{\pi}{4} * \left(0.95 * (ID_{PB})^2 + 0.005 * \left(ID_{TJ}\right)^2\right) \quad \text{Eq.22}$$

Centrifugal Body Forces due to Pipe Rotation

In general, for any axisymmetric body rotating around its axis of revolution there is a centrifugal body force created by the effect of angular velocity, **Figure 7**. In the case

of steady angular velocity, the body force is in the radial direction (i.e. normal to the pipe) and has a magnitude:

$$F_c = \rho * r * \omega^2 \qquad \text{Eq.23}$$

This occurs since the centrifugal body force is normal to the pipe. The resulting friction component is therefore:

$$F_t = \mu * \rho * r * \omega^2 \qquad \text{Eq.24}$$

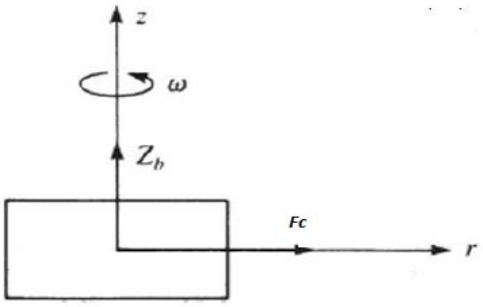

Figure 7: Axisymmetric Centrifugal Force

CHAPTER III

STRESS AND STRAIN TENSOR THEORY AND APPLICATION FOR DRILL PIPES

The Stress Strain Tensor Relationship

The representation of the stresses at the portion of pipe subject to study helps identify the normal forces and tangential forces (shear forces) acting on the pipe. This allows identification of the forces that contribute to torque and drag and the strains resulting from these stresses.

For a rigid material the stress and strain are related through the stiffness matrix, the general equation is:

$$\sigma^* = C^*.\epsilon^* \qquad \text{Eq.25}$$

Applying Stress Tensors over a Pipe Portion

The stress tensor at a certain point in the surface of the pipe is expressed in the following matrix form:

$$S = \begin{pmatrix} \sigma_{xx} & \sigma_{xy} & \sigma_{xz} \\ \sigma_{yx} & \sigma_{yy} & \sigma_{yz} \\ \sigma_{zx} & \sigma_{zy} & \sigma_{zz} \end{pmatrix} \qquad \text{Eq.26}$$

Normal Stress

Stress is by the definition the force divided by area on which the force is applied. Considering a force applied at a face of the element represented in **Figure 8**, the normal component of this force give rise to a normal stress, which is numerically obtained by dividing the normal component of the force by the area of the face on which it acts.

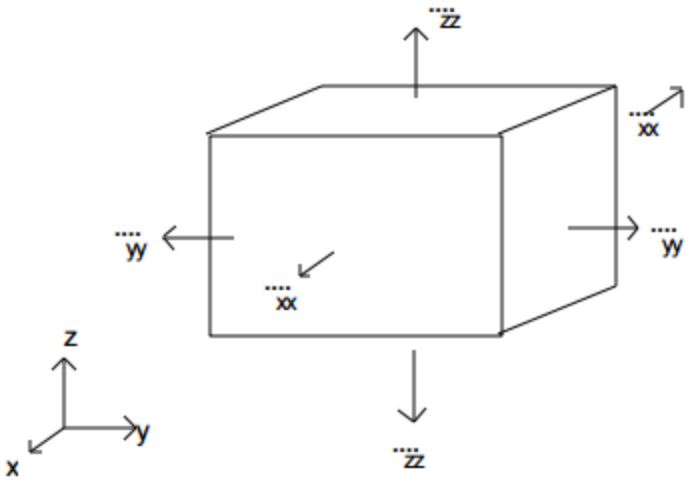

Figure 8: Illustration of Normal Stresses Directions and Notations

Shear Stress

Shear stress is the component of stress coplanar with the material cross-section, the force vector component parallel to the surface subject to the force gives rise to shear stress.

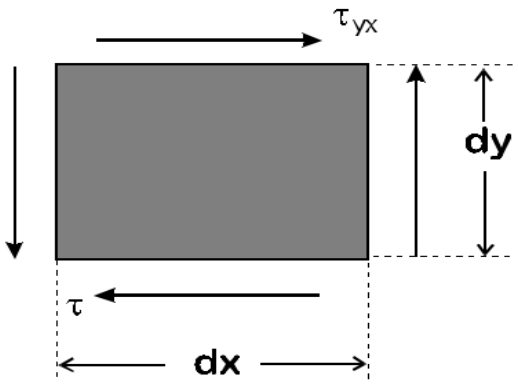

Figure 9: Shear Stress Orientation with regard to the Surface Subject to Force

Shear stress is obtained numerically in the same way normal stress is obtained, i.e. - by dividing the coplanar element of the force by the surface area, **Figure 9**.

The stress notation follows the standard conventions. For example σ_{xy} is the stress applied at the plane normal on the X-axis and in the direction of Y-axis. The force generating that stress has the same orientation in the plane (x, y, z) and is applied to the surface of the body normal to the axis X.

Stiffness Tensor

The stiffness tensor for a thick walled cylinder in the cylindrical coordinate system is shown in **Eq.27**:

$$C^* = \frac{E}{(1+v)(1-2v)} \begin{bmatrix} 1-v & v & 0 & 0 \\ v & 1-v & 0 & 0 \\ 0 & 0 & 1-v & 0 \\ 0 & 0 & 0 & 0.5-v \end{bmatrix} \quad \text{Eq.27}$$

E being Young's modulus, and v Poisson's ratio.

Principal Stresses and Cylindrical Coordinates

At every point in a stressed body there are at least three planes, called principal planes, with normal vectors **n** called principal directions, the stresses applied to the surface along the principal directions are perpendicular to the plane along the normal vector **n** and where there is no shear stresses τ_n. Consequently, the three stresses normal to these principal planes are called principal stresses.

The stress tensor being a physical quantity, it is independent of the coordinate system chosen to represent it, although the components σ_{ij} of the stress tensor depends on

the orientation of the coordinate system. Just like a vector for example which is a tensor of rank 1 in a three dimensional space, that tensor has three components that depend on the coordinate system in which it is chosen to represent the vector. The magnitude of the vector however is a physical quantity (a scalar) and it is independent of the Cartesian coordinate system or any other coordinate system for that matter. Similarly the stress or strain tensors components depend on the coordinate system they are represented in, they have three independent invariant quantities associated with it. One set of such invariants are the principal stresses of the stress tensor, which are just eigenvalues of the stress tensor. Their direction vectors are the principal directions or eigenvectors.

The principal stress tensor has therefore the following form:

$$\sigma^* = \begin{bmatrix} \sigma_1 & 0 & 0 \\ 0 & \sigma_2 & 0 \\ 0 & 0 & \sigma_3 \end{bmatrix} \quad \text{Eq.28}$$

In the case of a cylindrical shaped pipe the principal stresses direction coincides with the cylindrical local coordinate systems (r, θ, z)

Proposed Model: Stress-Based for Thick-Walled Cylinders

Coordinates Convention and Stress Expression

Typically for a thick walled cylinder the conventional (r, θ, z) cylindrical system of axis with regard to (x, y, z) Cartesian system of axis have configuration shown in **Figure 10**.

In order to be consistent with equations established in the drilling industry for torque and drag contributing forces. The convention shown in **Figure 10** was changed by

permuting the x-axis with the z-axis in the Cartesian convention. This new convention will be adopted in the following calculations when establishing the formulas for forces and stresses in cylindrical coordinates system of axis. Moreover, the choice of the cylindrical system of axis is preferable because of the simplicity it provides for expressing the stiffness matrix.

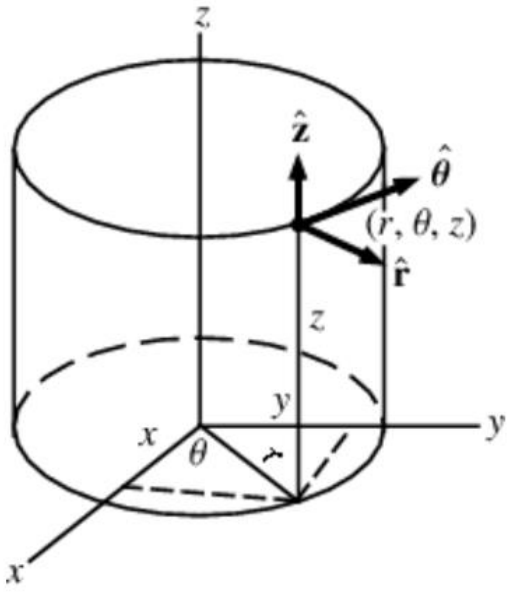

Figure 10: Cylindrical and Cartesian System of Axis Representation on a Cylinder

The stresses on the x-axis and z-axis in Cartesian coordinates will be identical to the stresses in the radial direction and z-axis in the cylindrical convention. **Figure 11** emphasizes these relative orientations.

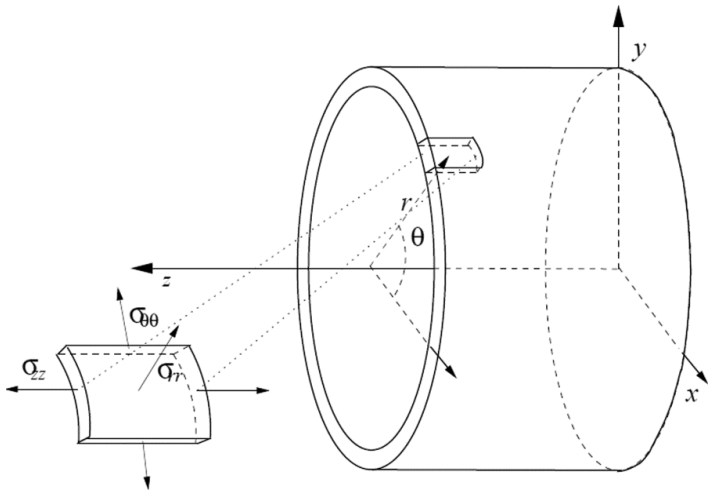

Figure 11: Direction of Stresses in the Cylindrical Coordinates relatively to the Cartesian Coordinates

Example Application to an Inclined Drillpipe Section

Let (x,y,z) be the coordinate system illustrated in the **Figure 12**. The diagonal components of the stress tensor being the normal stress applied on the portion of pipe subject of study and the off diagonal components are the shear stress components.

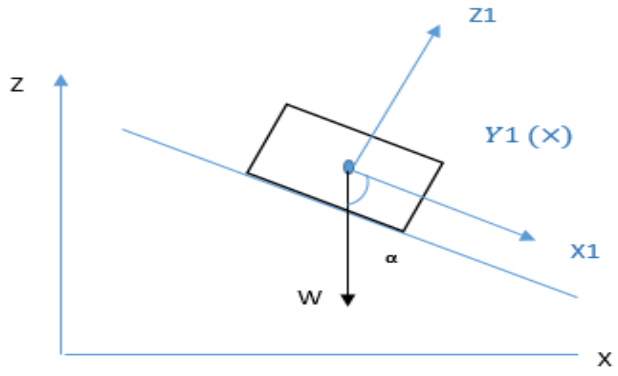

Figure 12: Force Balance Acting on a Portion of Drillstring

Based on this convention the stress is attributed to the weight of the portion of pipe studied as follows:

The pipe weight:

$$W_{xx} = W * \cos\alpha \quad \text{Eq.29}$$

Therefore,

$$\sigma_{xx} = W_{xx}/S_x \quad \text{Eq.30}$$

With S_x the Cross-sectional area of the pipe:

$$S_x = \frac{\pi}{4}(OD^2 - ID^2) \quad \text{Eq.31}$$

Similarly:

$$W_{zz} = W * \sin\alpha \quad \text{Eq.32}$$

And

$$\sigma_{zz} = W_{zz}/S_z \quad \text{Eq.33}$$

$$\sigma_{yy} = W_{yy}/S_y \quad \text{Eq.34}$$

With S_z, S_y , are the circumferential area of the drillpipe portion of length L:

$$S_z = S_y = \pi * OD * L \quad \text{Eq.35}$$

Using the same concept, we can obtain the shear stresses acting on the body subject of study in the (x, y, z) Cartesian coordinate system

The term accounting for well azimuth was dropped from the following equations because the forces balance was applied in the local system of axis, nonetheless this term will reappear in the stress transformation matrix.

Summarizing forces resulting in stresses we obtain:

Forces resulting in stressσ_{zz}:

$$F_z = W_b * \sin\alpha \qquad \text{Eq.36}$$

Forces resulting in stressσ_{xx}:

$$F_x = W_b * \cos\alpha \qquad \text{Eq.37}$$

Forces resulting in stressσ_{zx}:

$$F_{zx} = F_{xz} = \frac{1}{2} * C_D * (\rho * \mu_0^2 * d - \rho * \mu_1^2 * d_e) - \mu * (W_b * \sin\alpha * \sin\varphi) \qquad \text{Eq.38}$$

Given the cylindrical shape of the pipe and the orientation of the forces established above, the rest of the stresses in the stress tensor are eliminated and therefore:

$$F_y = F_{yz} = F_{xy} = 0 \qquad \text{Eq.39}$$

The stress tensor therefore is:

$$\begin{bmatrix} F_x & F_{xy} & F_{xz} \\ F_{xy} & F_y & F_{yz} \\ F_{xz} & F_{yz} & F_z \end{bmatrix} =$$

$$\begin{bmatrix} W_b * \cos\alpha / S_x & 0 & (\frac{1}{2} * C_D * \rho * \mu_0^2 * d - \frac{1}{2} * C_D * \rho * \mu_1^2 * d_e - \mu * W_b * \sin\alpha * \sin\varphi)/S_z \\ 0 & 0 & 0 \\ (\frac{1}{2} * C_D * \rho * \mu_0^2 * d - \frac{1}{2} * C_D * \rho * \mu_1^2 * d_e - \mu * W_b * \sin\alpha * \sin\varphi)/S_z & 0 & W_b * \sin\alpha / S_z \end{bmatrix} \quad \text{Eq.40}$$

Methodology of Calculations

Similar to the stiff string or soft string T&D models, the method of T&D calculation using stress-strain tensors starts from the bottom of the drill string and works its way upward until reaching the surface or until it reaches the depth of interest. The zone of interest is the depth where potential buckling can be anticipated, and where better design in regards to T&D is needed. Calculations can be also carried to the surface to determine the surface readings of torque and hookload.

If the bottom of the drill string is subject to the stress tensorσ_{ij0}, the strain inflicted by that stress tensor on the drill string segment 0 is obtained as follows

$$\epsilon_0{}^* = \mathrm{C}^{*-1}.\sigma_0{}^* \qquad \text{Eq.41}$$

It is important to stress that at each segment, when calculating the stress tensor, only the forces applied to that particular segment should be accounted for. Therefore, when calculating the forces applied to that segment, it should be considered as an isolated body, not subject to any tension or compression. Because the effect of the tension or compression is already accounted for in the stress tensor of the previous segments and will be added to the stress inflicted by the local forces on the current segment.

The same calculation is performed over the next segments. Starting from the local stress and working our way upwards. At segment u, the cumulative stress is the sum of the stresses from the preceding segments taking into account tortuosity effect on axis systems on this operation, as it will be shown in the next section.

The equivalent strain is therefore:

$$\sigma_{eq}{}^{*} = \sum_{k=0}^{u} \sigma_{k}{}^{*} \quad \text{Eq.42}$$

By reversing the same method of calculating stress tensor from forces, we can calculate the cumulative forces applied at an element of drillstring.

An important feature during the design is to compartmentalize the drill string into a finite number of segments. Many parameters should be taken into consideration while doing so, including, the length of each segment, the change in inclination and azimuth from one segment to the next, the change in pipe diameter and thickness from one segment to the next. For example, a drill pipe and a drill collar should not be in the same segment because they have different diameters and stiffness and that will cause the stress to be unequally partitioned along the segment. The segment has to be fairly straight, This feature is especially important at angle build up regions in directional wells or in high tortuosity horizontals, as the angular deviation amplifies the strain transmission from underneath to top segment with high concentration on the inside arc.

Inclination, Azimuth and Tortuosity Angular Effect

Changes in well trajectory will occur whether planned for or not. These changes affect the amount of stress transmitted from one segment to the next. Whether it is a change in well inclination or well azimuth the relation between the new stress tensor in terms of the old stress tensor in 2-D is given by the following formula:

$$\sigma_{new} = T^{*}.\sigma_{old}{}^{*} \quad \text{Eq.43}$$

In 3-D case the relation becomes

$$\sigma_{new} = T^{*}.\sigma_{old}{}^{*}.T^{*t} \quad \text{Eq.44}$$

2-D Transformations

In the case of a change in well inclination without change in well azimuth, and letting θ be the angle between segment i and segment i+1. Since the change is only in well inclination, the transformation is only a 2-D transformation as it is shown in the next figure.

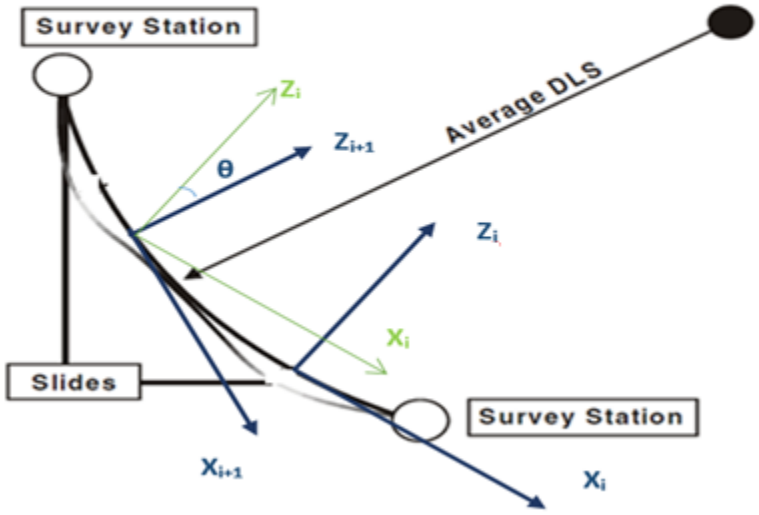

Figure 13: 2-D Angle Transformation of Local Coordinate's Axis

A change in well inclination or well azimuth exclusively will result in a 2-D transformation of the local coordinates system of axis. In the case illustrated in **Figure 13**, only axis-x and z are rotated with an angleθ, axis-y remains unaffected by the change of angle.

The transformation matrix relates the stress expressed in the old coordinates axis and the new coordinates axis. When stress is expressed in the local Cartesian coordinates system,

the transformation matrix for the new stress in terms of the old is a function of the angle θ as follows:

$$T^* = \begin{bmatrix} \cos\theta^2 & sin\,\theta^2 & 2\sin\theta\cos\theta \\ \sin\theta^2 & \cos\theta^2 & -2\sin\theta\cos\theta \\ -\sin\theta\cos\theta & \sin\theta\cos\theta & \cos\theta^2 - \sin\theta^2 \end{bmatrix} \quad \text{Eq.45}$$

For all practical reasons it is recommended to take θ as the angle determined by well trajectory survey (Inclination or azimuth). Therefore, it is a real time value that can be integrated in the equations in real time to adjust for new and corrected torque and drag values.

General Approach for 3-D Transformation

In the general case, a different approach to strain or stress transformation equations can give the expression of the transformation matrix. This approach is more complex but capable of generating an easy extension of the previous formula to 3-D.

For any random axis transformation in three dimension, the use of "Euler Rotation Theorem" can lead to the expression of the matrix of transformation with the simple use of transformation trigonometric.

This method sums the process of obtaining the new axis from the old axis in three steps as it is shown in **Figure 14**.

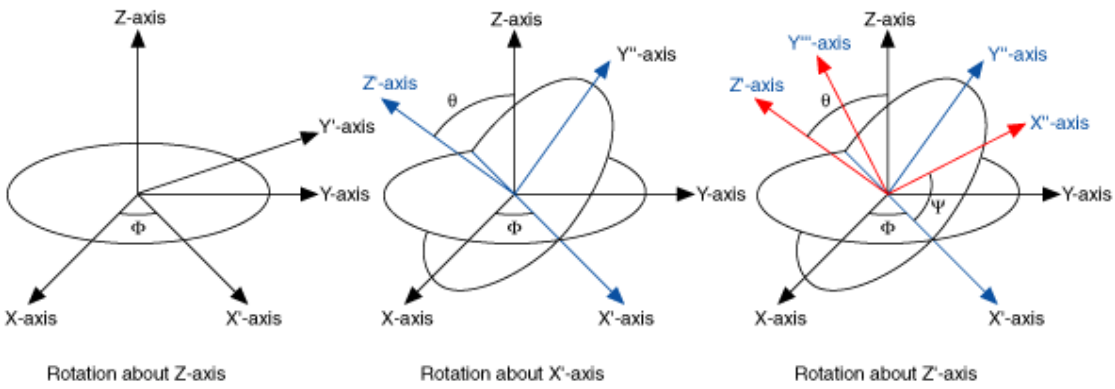

Figure 14: Transformation in terms of Euler Angles

The first step consists of rotating the original (x, y, z) axes by an angle ψ around the z-axis to obtain a new frame we may call (x', y', z). The second step is to rotate this new frame by an angle θ about the x' axis to obtain another frame we can call (x', y'', z'). Finally, by rotating this frame by an angle φ around the z' axis to obtain the final frame (x''-y'''-z'). These three transformations correspond to the transformation matrix

$$T^* = \begin{bmatrix} \cos\psi & \sin\psi & 0 \\ -\sin\psi & \cos\psi & 0 \\ 0 & 0 & 1 \end{bmatrix} \begin{bmatrix} 1 & 0 & 0 \\ 0 & \cos\theta & \sin\theta \\ 0 & -\sin\theta & \cos\theta \end{bmatrix} \begin{bmatrix} \cos\varphi & \sin\varphi & 0 \\ -\sin\varphi & \cos\varphi & 0 \\ 0 & 0 & 1 \end{bmatrix} \quad \text{Eq.46}$$

Pipe Buckling

The behavior of the string under compressive stress depends on the magnitude of the latter. As long as the compression is below the critical value, the string will sustain the compression without buckling. Above the critical value of compression, the string will buckle in a sinusoidal form. Above the helical buckling critical load, the pipe will no longer conserve its snaky configuration and will coil up against the wellbore and helically

buckle. Due to the immediate dramatic increase in wall force in the case of helical buckling, string lock up will follow immediately after helical buckling

Typical buckling behavior in an ERD-type well profile is shown in **Figure 15**. Only the upper portion of the 80° tangent section is shown where compression exceeds the critical buckling load. Buckling extends from the 80° tangent, where compression is a maximum up into the near-vertical section. In the 80° section, stabilization forces due to high inclination provide adequate support to restrain the buckling to the sinusoidal mode. In the build section, wellbore curvature provides additional support restraining the buckling in that section to the sinusoidal mode and of less severity than the 80° tangent section. Full helical buckling develops in the near-vertical section where the string receives little support from the wellbore. This helical buckling gradually disappears as the neutral point is approached where compression in the string is less than the critical buckling load.

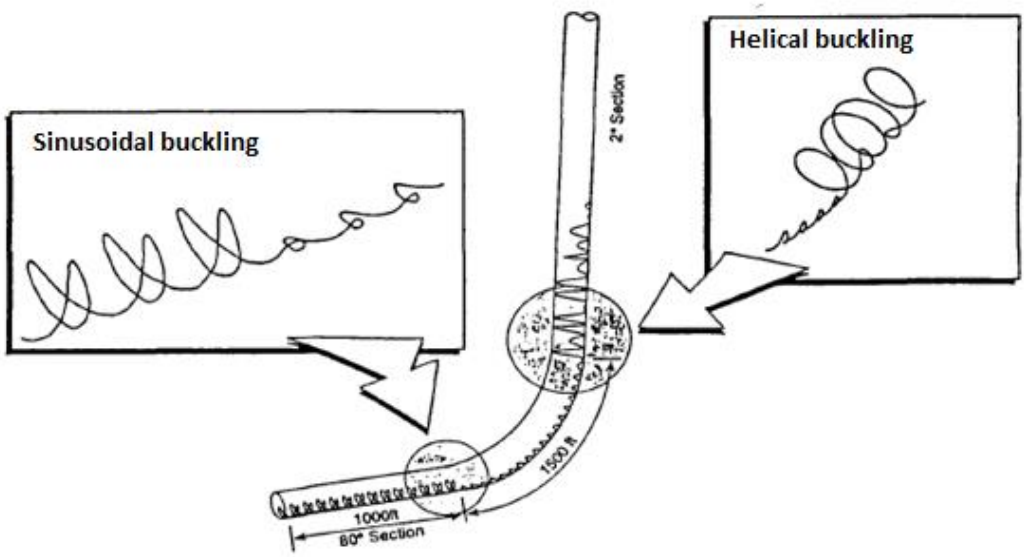

Figure 15: Zones of Potential Buckling in Directional Wells (Payne, M. L. et al, 1996)

Under increasing compressive stress the pipe might buckle if the normal compressive stress exceeds a yield criterion

Figure 16: Buckling Onset Stress

In **Figure 16**, Euler's buckling analysis sets the critical load that onsets sinusoidal buckling of a pipe:

$$W = \frac{\pi^2 EI}{L^2} \qquad \text{Eq.47}$$

It is very important to understand that accurate buckling prediction relies on accurate drag estimation first and for most. The analysis that will yield the buckling onset compressive force would account for tubulars radius and stiffness, hole size, and drill string clearance. Therefore, it is very important to properly model torque and drag in order to predict buckling zones accurately.

CHAPTER IV

FIELD CASE AND MODEL SIMULATION

Introduction to the Example Well

The well that has been selected for the new model simulation and comparison with real T&D data, is a horizontal well drilled in Texas from a land rig to a TD of 10926 ft. The directional section with angle build-up starts at MD of 6118 ft and reaches the horizontal section at MD of 7340 ft. **Figure 17** and **Figure 18** shows the inclination and azimuth profile vs MD.

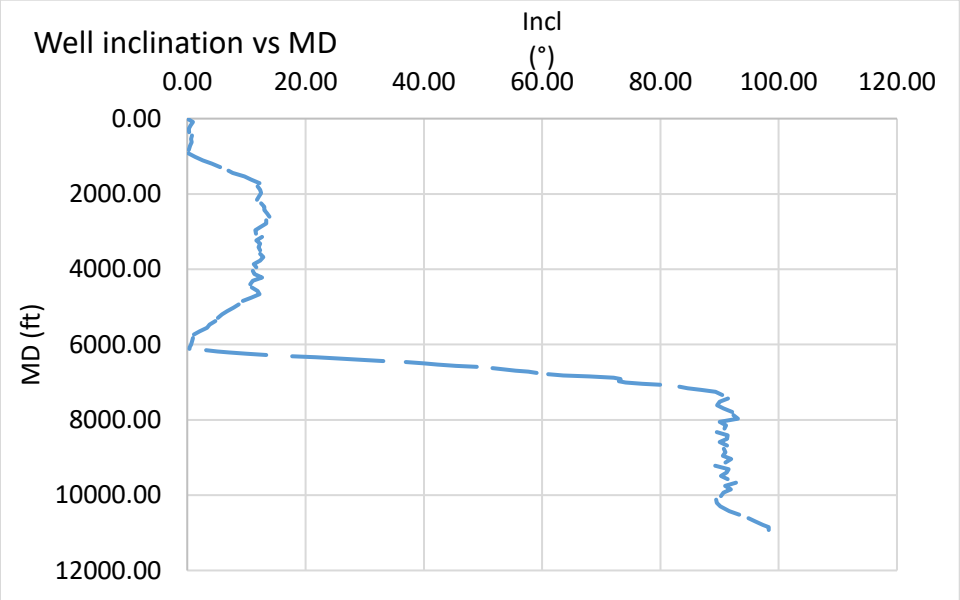

Figure 17: Example Well Inclination Profile vs MD

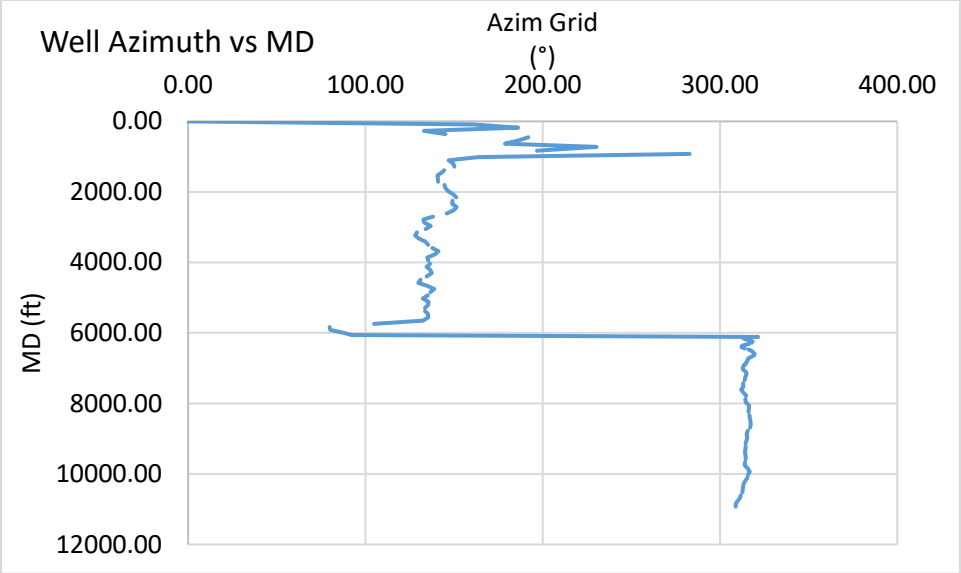

Figure 18: Example Well Azimuth Profile vs MD

Figure 19 shows the hookload plotted vs MD of both cases P/U and S/O for the following cases:

- Theoretical string weight
- Actual string weight
- P/U theoretical case with FF from 0.1 to 0.5
- Actual P/U weight
- S/O theoretical case with FF from 0.1 to 0.5
- Actual S/O weight

Figure 19 also lists the well characteristics, hole profile, string composition, mud weight, and casing depth, as well as the location of the zones studied.

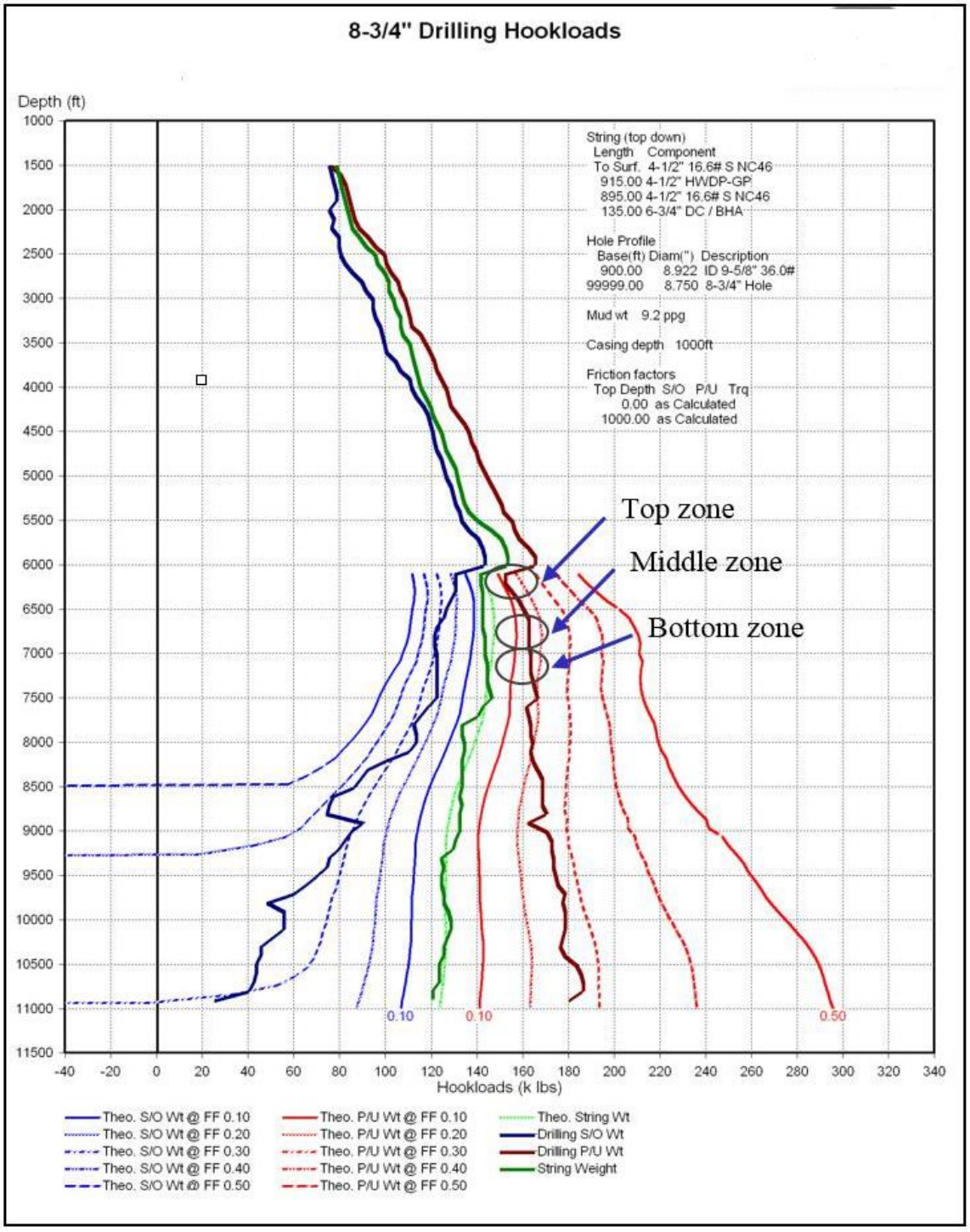

Figure 19: Example Well P/U and S/O Hookload vs MD, and Theoretical and Actual String Weight

Figure 19 presents the plots of hookload vs measured depth, the light red curves are pull-up hookload prediction for friction factors ranging from 0.1 to 0.5 and the maroon curve is the actual pull-up hookload vs MD. The light blue curves are slack-off hookload vs MD predicted for friction factors from 0.1 to 0.5, and the dark blue is the actual slack-off hookload vs MD. The light green curve is the theoretical rotating string weight and the dark green curve is the actual rotating string weight

Simulation Shows S&S Method Predicts Higher Drag Forces

Three zones of the directional section of the well were selected to run a simulation of drag forces using the proposed model. The upper zone is located in the directional section of the well near the vertical. The inclination in this zone is small, which makes the pipe weight contribute less to the normal force applied to the string, and therefore results in less friction and thus drag. In this zone Johancsik model provided relatively accurate predictions. S&S model provided also accurate predictions for this zone, which proves that when Johancsik model was accurate in this zone S&S was also accurate in predicting drag. The middle zone is where the gap between Johancsik prediction and actual drag is at a minimum. In this zone, it was critical to run our model in order to assess its ability to part away from Johancsik predictions and provide more accurate drag even when the gap was small. From the middle zone to the bottom zone, the gap between Johancsik prediction and actual drag gains in magnitude. S&S prediction for this section was increasingly far from Johancsik and close to actual data. The results from the three zones were compared

to drag forces calculated using Johancsik's model. The zones are listed in **Table 1**, and the results comparing the methods are illustrated in **Figure 20, Figure 21 and Figure 22**

Zone location	MD
Top zone	6309 ft-6404 ft
Middle zone	6787 ft- 6881 ft
Bottom zone	7116 ft- 7251 ft

Table 1: Zones Simulated in the Directional Section of the Example Well

The simulation and comparison were run for the case of P/U with FF=0.1 for each zone, the simulation assumed the string in that zone was divided into four segments which are drill pipes, and the transition from one segment to the next is the tool joint. This segment breakout allows to account for the tool joint circumference and cross-section when evaluating the stress tensors and driving drag for each segment. Drag forces for the zones in **Table** 1 were generated for both Johancsik model and S&S proposed model. **Figure 20**, **Figure 21**, and **Figure 22** show the results of the simulation and the comparison of the two models. As it can be seen from **Figure 20**, the predicted drag forces in the top zone from Johancsik model and the proposed model are almost identical in this section. As the inclination increases, the drag forces predicted by the new model show higher values than the forces predicted by Johancsik model as shown in **Figure 21**

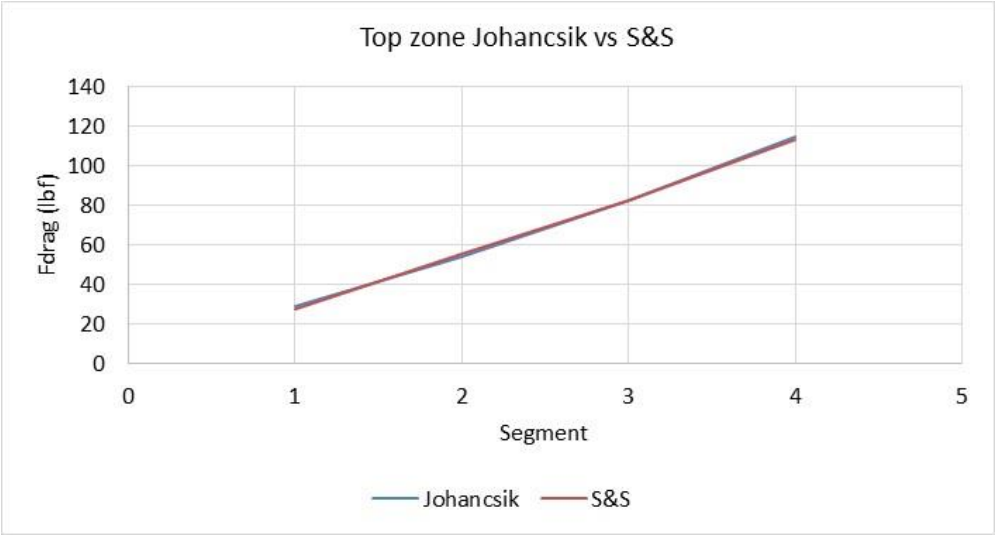

Figure 20: Drag Forces Simulated for the Top Zone Using Johancsik Model and the Proposed Model Show Minimal Differences between the two Methods.

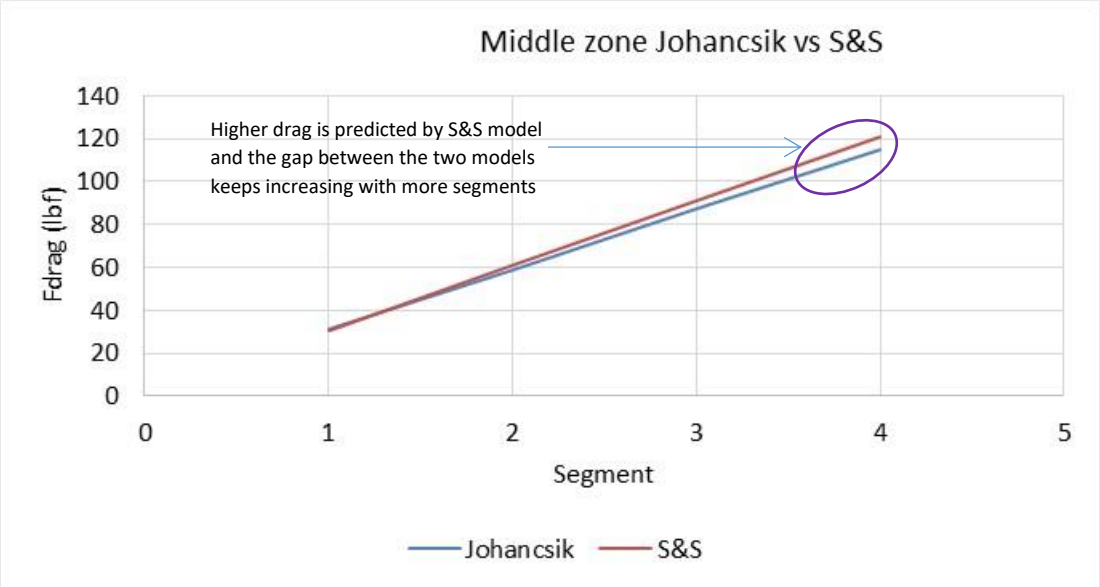

Figure 21: Drag Forces Simulated for the Middle Zone Using Johancsik Model and the Proposed Model Show Increasingly Higher Drag Using S&S Model Compared to Johancsik Model

The gap between the two models continues to build up with MD and well inclination as can be seen with it further increasing in bottom zone (**Figure 20**).

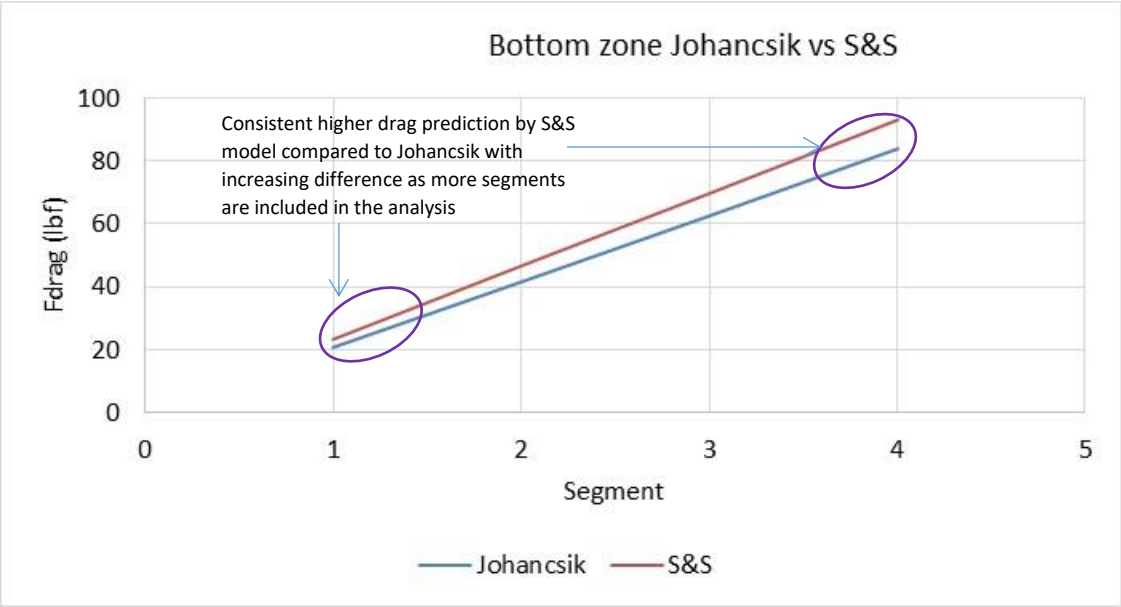

Figure 22: Drag Forces Simulated for the Bottom Zone Using Johancsik Model and the Proposed Model Showing Consistent Higher Prediction by S&S Model

Comparison of Models to Actual Drag Data

In order to quantify the discrepancy between theoretical and actual data and compare it to the gap between Johancsik model and the new model, an evaluation of the difference ratio was conducted for each case using the simulation results and the well data.

First, we define the difference ratio as the gap between two readings at the same depth divided by actual reading. Hence, the difference ratio between Johancsik drag and actual data is:

$$R_{\text{Difference}} = \frac{\text{Actual drag} - \text{Johancsik drag}}{\text{Actual drag}} \qquad \text{Eq.48}$$

Similarly the difference ratio between S&S model and actual readings is defined as:

$$R_{Difference} = \frac{\text{Actual drag} - \text{S\&S drag}}{\text{Actual drag}} \qquad \text{Eq.49}$$

The results of difference ratio for each one of the zones studied are provided in **Table 2**.

	Between actual drag and		
Difference ratio		S&S model	Johancsik model
	Top zone	1.64%	2.47%
	Middle zone	2.54%	3.82%
	Bottom zone	3.16%	5.38%

Table 2: Drag Difference Ratio Comparison between Johancsik/Actual and Johancsik/S&S Results

Discussion of Simulation Results

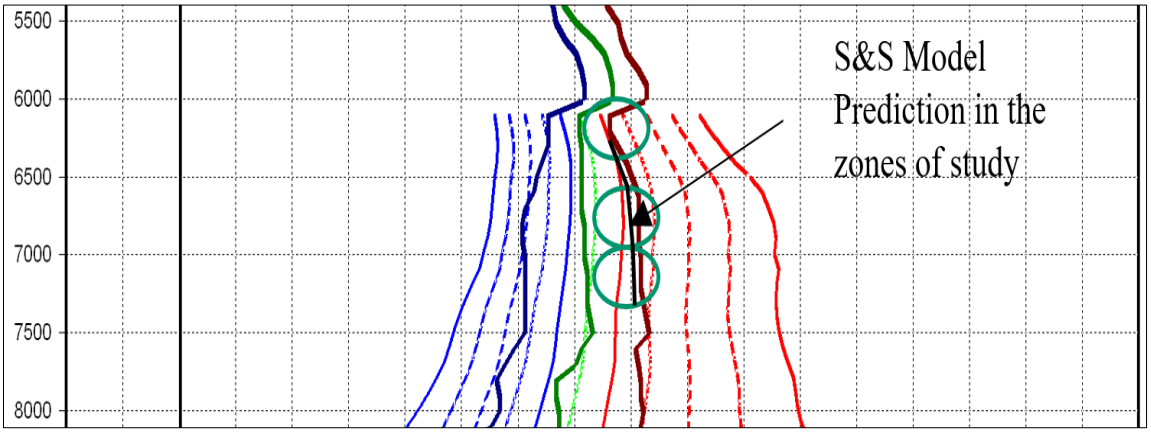

Figure 23: S&S Model Drag Prediction in the Middle and Bottom Zones, S&S Provided Higher Drag Prediction than Johancsik Model and Closer to Actual Data

Figure 23 shows that in the top zone the actual hookload and the Johancsik-based model, using a FF of 0.1, are almost identical. The difference ratio (Actual/Johancsik) was 2.5%, while the difference ratio (Actual/S&S) models was 1.6%. Therefore, the new S&S

model eliminated 64% of the error between Johancsik model and actual drag in the case of FF=0.1, better predicting the drag.

In the middle zone, a more considerable gap is seen between the Johancsik-based model hookload and the actual. The difference ratio (Actual/Johancsik) for this case was 3.8%, and the difference ratio (Actual/S&S) was 2.5%. The S&S model was able to predict higher drag and eliminate more than 60% of the original error (Actual/Johancsik).

Finally, in the bottom zone, a bigger gap can be seen between theoretical and actual hookloads. The difference ratio (Actual/Johancsik) for this case was 5.4%, while the difference ratio (Actual/S&S) was 3.16%. The actual hookload in the bottom zone is closer to the theoretical P/U case that uses a FF of 0.2 than the case with FF of 0.1. This represents one of the major drawbacks of Johancsik model, because the FF needs to be constantly adjusted and increased in curved sections and horizontals in order for Johancsik predicted data to match the field observed data. In middle zone as an example, the S&S model has been able to close this gap to less than 44% of its original magnitude between Johancsik and actual data, without the need to alter the FF used in the simulation.

Friction Factor		S&S model	Johancsik model
	Top zone	0.1	0.1
	Middle zone	0.112	0.145
	Bottom zone	0.128	0.182

Table 3: FF Used to Provide a Better Match of S&S Model and Johancsik Model to Actual Drag

In order to relate the simulation results to the common practices in T&D modeling, we assessed the FF needed to input in both models to provide better match to actual drag,

the results are shown in **Table 3**. Better match to actual drag of Johancsik prediction was achieved in the middle zone by increasing the FF to 1.145, and to 1.182 in the bottom zone, whereas better match of S&S model was obtained by increasing the FF to 1.112 only in the middle zone and to 1.128 only in the bottom zone.

S&S Model Advantages and Value

From figures 20, 21, and 23, S&S model was able to predict higher drag compared to Johancsik model and bring the prediction closer to actual drag. S&S model was able to narrow Johancsik prediction errors to less than 40% of its original magnitude. As it is shown in **Table 3**, the remaining error in S&S model prediction was overcome by slightly altering the FF by 0.012 in the middle zone, and 0.028 in the bottom zone. Thus reducing drag prediction dependency on FF compared to the changes this parameter was subject to when using Johancsik model.

The availability of survey data makes a big difference in Johancsik model prediction. In the top and middle zone, the simulation was run using one survey point every 30 ft, whereas in the bottom zone, only one survey point was available every 57 ft to 60 ft. This has driven Johancsik model to build more error in its prediction for the bottom zone compared to the top zones, and shows that Johancsik model is sensitive to survey point. S&S model consistently and evenly narrowed the error between the prediction and the actual data for both cases: one survey point every 30 ft and as well for the case of one survey point every 60 ft. Most of current models for T&D require a relatively short segment to accurately account for tortuosity, yet S&S model seem to perform evenly in short segments and what would be considered long segments for most

current T&D models. In Johancsik model, the hole size establishes limits with regard to segments length because of the beam bending equations used in it. A good survey interpolation between the available data points and the segment length would allow to carry the prediction with an estimated set of survey point, but such an interpolation would be very hard to establish and mimic realistically the inclination and azimuth in the zone of interest. S&S model was able to predict more accurate drag without the need of survey data interpolation, and therefore is not as sensitive as Johancsik model for this feature.

Although the last feature is an advantage for S&S model over Johancsik model, it would be a disadvantage in the presence of high dogleg severity. S&S model might omit the effect of high dogleg severity if the segments length is long enough to hide this feature.

Future Work

The present work laid the concept and basics of calculation for the new model to calculate torque and drag, and provided a simulation for a field case in order to assess different data to johancsik model. Nonetheless, in order to run a more accurate comparison between any software used in industry and the model derived in this work, the stress tensor for each segment has to be populated with the same forces accounted for in the software, especially with regard to pipe tension forces and axial loads. The forces have to be carefully attributed to their resulting stresses, forces resulting in normal stresses and forces resulting in shear stresses. Once the stress tensor of a course length segment is properly populated, a full-scale simulation for the integrity of the well can be run using a coded version of the S&S model. Since there will be a considerable number of segments and iterative matrices operations, it is recommended to code the present model in Matlab.

With a stress tensor populated with the same forces used in a software, and having the necessary data of well inclination and azimuth from surveys, a full-scale simulation from bottom to top of the well can be run, and then compared to actual T&D profiles and predictions using Johancsik model.

CHAPTER V

CONCLUSIONS AND RECOMMENDATIONS

The primary disadvantage of Johancsik model for T&D modeling is that it requires large changes of FF, which are in many cases difficult to predict, especially in curved sections of the well and laterals. The fact that companies alter this parameter in a purely empirical manner to match the observed field data without a precise physical explanation can be dangerous. Moreover, even if this process of FF calibration can improve T&D predictions in the Johancsik model using trial and error and field data matching, it remains very difficult to predict in new fields without offset well data, where such correlations cannot be conducted at least for the few first wells.

In stiff tubulars such as drill pipes and BHAs it is more physically representative to consider stress instead of discrete forces when studying T&D. The use of stress transformations matrices is also a better representation of geometry in the equations compared to the angular approximations in Johancsik equations. The major advantage of S&S model proposed in this work is the reduction of FF correction dependency, a better match to actual data was obtained by slightly altering the FF in the S&S model compared to the magnitude of change needed for the FF in Johancsik model. In the case study presented, the S&S still under-predicted the drag values but with 60% lesser gap compared to Johancsik model for a FF of 0.1.

NOMENCLATURE

T&D	Torque and Drag
S&S	Stress and Strain
WOB	Weight On Bit
ERD	Extended Reach Directional
BHA	Bottom Hole Assembly
TJ	Tool Joint
lb	pound
ft	feet
W_b	buoyed weight in lb/ft
W_a	adjusted weight of the pipe in air in lb/ft
ppg	Pound per gallon
MW	mud weight in ppg
W_{fluid}	weight per foot of displaced fluid
A_E	external area of the pipe
A_I	internal area of the pipe
ρ	density of the material
R	radius of the pipe
ω	angular velocity of the pipe
W	Weight
FF	Friction Factor

MD	Measured Depth
TD	Total Depth
DC	Drill collar
P/U	Pull up
S/O	Slack off
DP	Drill pipe
SPE	Society of Petroleum Engineers

REFERENCES

Aadnoy, B.S., Fazaelizadeh, M., Hareland, G. “A 3-Dimensional Analytica Model for Wellbore Friction”, Journal of Canadian Petroleum Technology, 2010.

Aadnoy, B.S., Kaarstad, E., “Theory and Application of Buoyancy in Wells”, SPE/IADC 101795 presented ate the SPE/IADC Asia Pacific Drilling Technology Conference and Exhibition, Bankok, Thailand, November 2006.

Dawson, R. and Paslay, P.R. 1984. “Drill Pipe Buckling in Inclined Holes”. SPE Journal of Petroleum Technology 36 (10): 1734-1738. SPE-11167-PA.

Fazaelizadeh, M., Hareland, G., Aadnoy, B.S. “Application of New 3-D Analytical Modelfor Directional Wellbore Friction‖, Journal of Modern Applied Science”, Vol.4, No. 2, 2010

Gaynor, T., Chen, D.C., Stuart D., and Comeaux, B. 2001. “Tortuosity Versus Micro-Tortuosity – Why Little Things Mean a Lot”. Paper SPE/IADC 67818 presented at the SPE/IADC Drilling Conference, Amsterdam, The Netherlands, 27 February-1 March.

Gaynor, T., Hamer, D., Chen, D., “Quantifying tortuosities by Friction Factors in Torque and Drag Model‖”, SPE 77617, Annual Technical Conference and Exhibition, San Antonio, Texas, September, 2002.

Johancsik, C.A., Friesen D.B., Rapier Dawson “Torque and Drag in Directional Wells-Prediction and Measurement”, June 1984, SPE-11380-PA

Kyllingstad, A. 1995. “Buckling of tubular strings in curved wells. Journal of Petroleum Science and Engineering” 12: 209-218.

Maidla, E.E., Wojtanowicz, A.K., “Field method of assessing borehole friction for directional well casing” SPE Middle East Oil Show, Manama, Bahrain, March, 1987.

Mirhaj, S.A., Fazaelizadeh, M., Kaarstad, E., Aadnoy, B.S. “New Aspects of Torque and Drag Modelling in Extended Reach Wells”, SPE 135719, SPE Annual Technical Conference and Exhibition, Florence, Italy, September 2010.

Mirhaj, S.A., Kaarstad, E., Aadnoy, B.S. "Minimizing Friction in Shallow Horizontal Wells", SPE 135812, IADC/SPE Asia Pacific Drilling Technology Conference and Exhibition, Ho Chi Minh, Vietnam, 1-3 November 2010.

Mitchell, R.F. and Samuel, R. 2009. “How Good Is the Torque/Drag Model?” SPE Drilling& Completion 24 (1): 62-71. SPE-105068-PA.

Payne, M.L. 1996. “Advanced Torque and Drag Considerations in Extended-Reach Wells” IADC/SPE 35102-MS.

Roylance David. “Transformation of Stresses and Strains”. Department of Materials Science and Engineering Massachusetts Institute of Technology Cambridge, MA 02139 May 14, 2001

Samuel, R. and Kumar, A. 2012. “Effective Force and True Force: What are They?” Paper IADC/SPE 151407 presented at the IADC/SPE Drilling Conference and Exhibition, San Diego, USA, 6-8 March.

Tang, W., Muradov, A., Chandler, R.B., Jellison, M.J., Prideco, G., Gonzalez M.E., and Wu, J. 2006. “A Novel Approach for Determining, Evaluating, and Applying Stress Concentration Factors for Rotary-Shouldered Connections”. Paper SPE 103052 presented at the SPE Annual Technical Conference and Exhibition, San Antonio, Texas, 24-27 September.

Wolfram Research http://scienceworld.wolfram.com/physics/CylinderDrag.html

Wu, J., and Juvkam-Wold, H.C. 1993. “Study of Helical Buckling of Pipes in Horizontal Wells”. Paper SPE 25503 presented at the Production Operations Symposium, Oklahoma City, Oklahoma, 21-23 March.